Disorders of the Nervous System

GSK3β Impairs KIF1A Transport in a Cellular Model of Alzheimer's Disease but Does Not Regulate Motor Motility at S402

K.J. Gan,[1] A. Akram,[1,*] T.L. Blasius,[4,*] E.M. Ramser,[2] B.G. Budaitis,[4,5] D.R. Gabrych,[1] K.J. Verhey,[4] and M.A. Silverman[1,2,3]

https://doi.org/10.1523/ENEURO.0176-20.2020

[1]Department of Molecular Biology and Biochemistry, Simon Fraser University, Burnaby, BC, V5A1S6, [2]Department of Biological Sciences, Simon Fraser University, Burnaby, BC, V5A1S6, [3]Centre for Cell Biology, Development and Disease, Simon Fraser University, Burnaby, BC, V5A1S6, [4]Department of Cell and Developmental Biology, University of Michigan Medical School, and [5]Program in Cellular and Molecular Biology, University of Michigan, Ann Arbor, Michigan, 94305

Abstract

Impairment of axonal transport is an early pathologic event that precedes neurotoxicity in Alzheimer's disease (AD). Soluble amyloid-β oligomers (AβOs), a causative agent of AD, activate intracellular signaling cascades that trigger phosphorylation of many target proteins, including tau, resulting in microtubule destabilization and transport impairment. Here, we investigated how KIF1A, a kinesin-3 family motor protein required for the transport of neurotrophic factors, is impaired in mouse hippocampal neurons treated with AβOs. By live cell imaging, we observed that AβOs inhibit transport of KIF1A-GFP similarly in wild-type and tau knock-out neurons, indicating that tau is not required for this effect. Pharmacological inhibition of glycogen synthase kinase 3β (GSK3β), a kinase overactivated in AD, prevented the transport defects. By mass spectrometry on KIF1A immunoprecipitated from transgenic AD mouse brain, we detected phosphorylation at S402, which conforms to a highly conserved GSK3β consensus site. We confirmed that this site is phosphorylated by GSK3β in vitro. Finally, we tested whether a phosphomimic of S402 could modulate KIF1A motility in control and AβO-treated mouse neurons and in a Golgi dispersion assay devoid of endogenous KIF1A. In both systems, transport driven by mutant motors was similar to that of WT motors. In conclusion, GSK3β impairs KIF1A transport but does not regulate motor motility at S402. Further studies are required to determine the specific phosphorylation sites on KIF1A that regulate its cargo binding and/or motility in physiological and disease states.

Key words: Alzheimer's disease; amyloid beta oligomers; axonal transport; glycogen synthase kinase beta; kinesin-3 (KIF1A); motor protein phosphorylation

---

Significance Statement

Axonal transport of proteins and organelles is required for neuronal function and survival and is impaired in Alzheimer's disease (AD). Pathogenic mechanisms that directly impact motor protein motility before neuronal toxicity have not been widely investigated. Here, we show that KIF1A, the primary kinesin motor required for transport of neurotrophic factors, is impaired in mouse neurons treated with amyloid-β oligomers (AβOs), a causative agent of AD. Inhibition of glycogen synthase kinase 3β (GSK3β), a kinase overactivated in AD, prevents these defects. We detected phosphorylation of S402, a highly conserved GSK3β consensus site, in KIF1A immunoprecipitated from AD mouse brain. However, a phosphomimic of S402 did not modulate KIF1A motility in cell-based assays. Thus, GSK3β impairs KIF1A transport but likely not through phosphorylation at S402.

Introduction

Neurons rely on microtubule-based, fast axonal transport of proteins and organelles for development, communication, and survival. Transport is driven by kinesin and cytoplasmic dynein motor proteins that carry cargoes anterogradely toward the synapse or retrogradely toward the cell body, respectively. Impaired motor-cargo binding and/or disrupted motor-microtubule interactions are common to several neurodegenerative diseases (Brady and Morfini, 2017). Importantly, they arise before neurite dystrophy, synapse loss, and cell death. In experimental models of Alzheimer's disease (AD), axonal transport of neuropeptide vesicles and mitochondria are perturbed by soluble amyloid-β oligomers (AβOs; Decker et al., 2010; Gan and Silverman, 2015; Seifert et al., 2016; Zhang et al., 2018), which accumulate in AD brain before detectable formation of Aβ plaques and neurofibrillary tangles (Ferreira et al., 2015). AβOs activate intracellular signaling cascades that lead to phosphorylation and aberrant activation of many target proteins, including the microtubule-associated protein tau (Cline et al., 2018). Although much research has focused on tau hyperphosphorylation and on subsequent microtubule destabilization and cytoskeletal collapse that halt transport in advanced stages of AD, it fails to account for earlier, subtler and potentially reversible mechanisms that modulate transport independent of tau. Thus, we focused our investigation on AβO-activated kinases that might directly impair motor protein activity.

AD-associated kinases phosphorylate kinesin-I (KIF5) and thereby impair motility and cargo binding (Gibbs et al., 2015; Brady and Morfini, 2017); however, it is unknown whether they regulate the kinesin-3 motor, KIF1A. KIF1A associates with several different membranous organelles such as dense core vesicles (DCVs), which contain critical signaling molecules including brain-derived neurotrophic factor (BDNF; Yonekawa et al., 1998; Lo et al., 2011; Kondo et al., 2012; Hung and Coleman, 2016).

Despite the importance of BDNF in neuronal physiology and its reduced availability in AD and other neurodegenerative diseases (Mariga et al., 2017), mechanisms that regulate its transport by KIF1A are unclear. Previously, Decker et al. (2010) demonstrated that AβOs impair axonal BDNF transport in primary hippocampal neurons. Contrary to a current model (Bloom, 2014), these transport defects are induced independent of tau, microtubule destabilization, and acute cell death (Ramser et al., 2013). Furthermore, in these studies, BDNF transport impairment was prevented by inhibiting glycogen synthase kinase 3β (GSK3β), a kinase that is implicated in many aspects of AD pathogenesis (Maqbool et al., 2016) and regulates kinesin-1 interactions with cargo and microtubules (Morfini et al., 2002; Weaver et al., 2013). Whether AβO-induced dysregulation of GSK3β signaling directly affects KIF1A motility has not been investigated.

Here, we show by live cell imaging that AβOs impair KIF1A motility in wild-type (WT) and tau knock-out hippocampal neurons, indicating that tau is not required for KIF1A transport disruption. Pharmacological inhibition of GSK3β prevents these defects, and GSK3β coimmunoprecipitates with KIF1A, indicating that this kinase may regulate motility. By mass spectrometry (MS) on KIF1A isolated from AD mouse brain, we identified several phosphopeptides targeted by kinases associated with AD, including GSK3β. We discovered that S402, located proximal to the neck-coil domain, conforms to a highly conserved GSK3β consensus site and hypothesized that it might regulate KIF1A processivity. Thus, we tested whether a phosphomimic of S402 could modulate KIF1A motility in mouse neurons and in a Golgi dispersion assay devoid of endogenous KIF1A (Engelke et al., 2016; Budaitis et al., 2019). In both systems, we did not observe any alterations in the motility of KIF1A. Further studies will be required to determine whether other phosphorylation sites on KIF1A regulate its motility or binding to DCVs in physiological and AD states.

Materials and Methods

Hippocampal cell culture and expression of transgenes

Primary hippocampal neurons from embryonic day (E)16 WT and tau knock-out mice of either sex (The Jackson Laboratory) were cultured as described previously (Kaech and Banker, 2006) and kept in PNGM primary neuron growth media (Lonza). The glial feeder layer was derived from murine neural stem cells as described previously (Miranda et al., 2012). At 10–12 d in vitro (DIV), cells were cotransfected using Lipofectamine 2000 (Invitrogen) with plasmids encoding soluble blue fluorescent protein (pmUβA-eBFP) and mouse KIF1A-GFP (GW1-KIF1A-eGFP; Lee et al., 2003). Cells expressed constructs for 36 h before live imaging of KIF1A transport. All experiments with animals were approved by and followed the guidelines set out by the University Animal Care Committee, Protocol 1261B-05.

AβO and GSK3β Inhibitor VIII treatments

Soluble, full-length Aβ 1–42 peptides (American Peptide) were prepared exactly according to the method of Lambert

et al., 2007 (Lambert et al., 2007) and applied to cells at a final concentration of 500 nM for 18 h. Cells were incubated with 5 μM GSK3β Inhibitor VIII (Calbiochem) or equivalent volumes of vehicle (EtOH) 30 min before AβO or vehicle treatment.

Live imaging and analysis of KIF1A transport

KIF1A-GFP transport was analyzed using a standard wide-field fluorescence microscope equipped with a cooled charge-coupled device camera and controlled by MetaMorph (Molecular Devices) as described previously (Kwinter and Silverman, 2009; Gan and Silverman, 2016). All imaging, typically 100 frames, was recorded by the "stream acquisition module" in MetaMorph. Briefly, cells were sealed in a heated imaging chamber, and recordings were acquired from double transfectants at an exposure time of 250 ms for 90 s. This captured dozens of transport events per cell in 100-μm segments of the axon. Dendrites and axons were initially identified based on morphology and confirmed retrospectively by immunostaining against MAP2, a dendritic cytoskeletal protein. Soluble BFP detection was necessary to determine the orientation of the cell body relative to the axon and thus to distinguish between anterograde and retrograde transport events. Motor protein flux, velocity, and run lengths were obtained through tracing kymographs in MetaMorph. Flux is the summation of distances traveled by all moving KIF1A puncta standardized by the length of axon imaged and duration of each movie (in microminutes): $\dfrac{\sum_{i=1}^{n} d_i}{l \times t}$ where d are the individual KIF1A run lengths, l is the length of axon imaged and t is the duration of the imaging session. A KIF1A punctum was defined as undergoing a directed run if it traveled a distance of $\geq 2\,\mu$m. This distance was determined as a safe estimate of the limit of diffusion based on the assumption that root-mean-squared displacement equals $\sqrt{2Dt}$, where D is the diffusion coefficient ($D = 0.01\ \mu$s^2/s for the KIF1A cargo of DCVs) and t is the duration of the imaging period ($t = 50$ s; Abney et al., 1999; Gan and Silverman, 2016). A run was defined as terminating if the vesicle remained in the same position for at least four consecutive frames. Percentage flux represents the flux in treated neurons normalized to controls (100%). Statistical analyses were performed using Microsoft Excel or GraphPad Prism. Data are presented as mean $\pm$ SEM. Significant differences between treatments were analyzed by t tests with equal or unequal variance at a 95% confidence interval. For live imaging experiments, a minimum of 15 cells from three independent cultures ($n = 3$) were analyzed.

KIF1A immunoprecipitation and GSK3β immunoblotting

Primary hippocampal neurons from E16 WT C57Bl/6 mice (The Jackson Laboratory) were lysed in ice-cold radioimmunoprecipitation assay (RIPA) buffer (50 mM Tris; pH 7.5, 5 mM EDTA, 150 mM NaCl, 1% Triton X-100) containing cOmplete protease inhibitor cocktail (Roche), Halt phosphatase inhibitor cocktail (ThermoFisher), 1 mM

phenylmethylsulfonyl fluoride (PMSF), and 1 mM orthovandate. A total of 500 μg of lysate was mixed overnight at 4°C with 12 μg of KIF1A antibody (BD Transduction Laboratories; catalog #612094). Samples were then combined with 50 μl of Protein A/G-agarose (Santa Cruz Biotechnology; catalog #sc-2003) beads and mixed at 4°C for 3 h. Samples were gently pelleted and rinsed three times with RIPA buffer. The immunoprecipitated proteins (5–10 μg) were resolved on 10% SDS-PAGE gels and transferred to polyvinylidene difluoride (PVDF) membranes. Membranes were probed with anti-KIF1A (1:1000, BD Transduction Laboratories; catalog #612094) and anti-GSK3β (1:000, Cell Signaling Technology; catalog #27C10) overnight at 4°C. Immunoreactive bands were visualized using enhanced chemiluminescent substrate (ThermoFisher Scientific) for detection of peroxidase activity from horseradish peroxidase (HRP)-conjugated antibodies.

To detect total KIF1A phosphorylation, C57Bl/6 adult mouse hippocampi (six) were homogenized and lysed in ice-cold RIPA buffer containing cOmplete protease inhibitor cocktail (Roche), Halt phosphatase inhibitor cocktail (ThermoFisher), 1 mM PMSF, and 1 mM orthovandate. 500 μg of lysate was mixed overnight at 4°C with 12 μg of KIF1A antibody (BD Transduction Laboratories; catalog #612094). Samples were then combined with 50 μl of Protein A/G-agarose (Santa Cruz Biotechnology; catalog #sc-2003) beads and mixed at 4°C for 3 h. Samples were gently pelleted and rinsed three times with RIPA buffer. The immunoprecipitated proteins (5–10 μg) were resolved on 10% SDS-PAGE gels and transferred to PVDF membranes. Membranes were probed with an anti-phosphoserine monoclonal antibody 7F12 (1:2000, Invitrogen) and an anti-phosphothreonine monoclonal antibody PT-5H5 (1:2000, Invitrogen) overnight at 4°C. Immunoreactive bands were visualized using enhanced chemiluminescent substrate (SuperSignal West Pico PLUS Chemiluminescent Substrate, ThermoFisher Scientific) for detection of peroxidase activity from HRP-conjugated secondary antibodies.

To determine the presence of KIF1A in COS7 cells, total protein isolated from cell lysates (15 μg) were separated on a precast 4–15% gradient gel (Bio-Rad Laboratories) and subsequently transferred to a PVDF membrane. Membranes were blocked using a 3% BSA solution in TBS-Tween and blotting was performed using primary antibodies in blocking solution against KIF1A (1:500; BD Transduction Laboratories) and the loading control, GAPDH (1:1000; Novus Biologicals; catalog #NB300-327). Immunoreactive bands were visualized using enhanced chemiluminescent substrate (SuperSignal West Pico PLUS Chemiluminescent Substrate: ThermoFisher Scientific) for detection of peroxidase activity from HRP-conjugated secondary antibodies. Blotting was performed in triplicate using two different cell lysate samples.

Tandem MS (MS/MS) and KIF1A phosphosite analysis

KIF1A was immunoprecipitated from 14-month-old Tg2576 AD (APPSwe) and age-matched WT control mouse brains that were provided by T. Tomiyama (Osaka City University, Japan). Cortices from three brains of each genotype were first homogenized in standard RIPA buffer

with 1% NP-40 including cOmplete protease inhibitor cocktail (Roche), Halt phosphatase inhibitor cocktail (ThermoFisher), 1 mM PMSF, and 1 mM orthovandate in a Retsch Mixer Mill 301. Lysates were cleared of insoluble material by centrifugation at 14,000 × g for 10 min at 4°C and then incubated with 3.5 μg of anti-KIF1A (BD Transduction Laboratories; catalog #612094) for 3 h at 4°C using constant rotation. Subsequently, 40 μl of Protein A/G PLUS–agarose beads (Santa Cruz Biotechnology; catalog #sc-2003) were added and incubated for another 3 h at 4°C using constant rotation. Immune complexes were washed with 1× RIPA with 0.5 M NaCl and pelleted, followed by a second wash using 2× RIPA with 140 mM NaCl. A total of 5 μg of each sample was heated to 95°C in 2× Laemmli buffer containing 100 mM DTT and resolved on a 10% SDS-PAGE gel. Coomassie-stained protein bands were excised from the SDS-PAGE gel, digested with trypsin, and used for MS/MS with TiO₂ enrichment for phosphopeptides (University of Victoria Genome BC Proteomics Centre). MS was performed twice on each sample. KIF1A phosphorylation from Tg2576 and WT brain were compared using the algorithm PhosphoRS, which calculates the probability of each phosphorylation site within a peptide. GSK3β phosphosites were identified by comparison to existing sequences within the Phosida (phosida.com) and Phosphonet (https://kinexus.ca) databases.

Details of MS protocol

In gel trypsin digestion

Gel slices were manually cut into 1-mm cubes and Coomassie Blue gel cubes de-stained (50/45/5 v/v methanol/water/acetic acid). Gel cubes were washed with water and 200 mM ammonium bicarbonate before reduction (10 mM dithiothreitol, Sigma) 30 min at room temperature and alkylation (100 mM iodoacetamide, Sigma) 30 min at room temperature. Modified sequencing grade porcine trypsin solution 30 μl (20 ng/μl, Promega) was added to the gel slice enzyme/protein ratio 1:50 and then digested for 16 h at 37°C. The peptides were extracted out of the gel slices with 400 μl (60/39/1 v/v acetonitrile/water/trifluoracetic acid). The sample was then speed vac centrifuged and stored at −80°C until analysis.

Titanium dioxide phosphopeptide enrichment

TiO₂ binding buffer [70% v/v acetonitrile, 5% v/v trifluoroacetic acid (TFA), containing 300 mg/ml lactic acid] was added to 80% of each sample digest along with 10 mg of TiO₂ beads (GL Science, 10 μm in diameter). Samples were incubated with TiO₂ with end-over-end rotation for 90 min at 25°C. After incubation, TiO₂ beads were transferred to homemade StageTip with C₈ frit for phosphopeptide elution. The beads were washed 4 × 50 μl TiO₂ binding buffer, and 4 × 50 μl buffer B (80% ACN, 0.1% TFA). Elution was performed with the following steps: 50 μl 0.5% NH₄OH, 50 μl 0.5% NH₄OH/30% ACN, and 50 μl 0.5% NH₄OH/50% ACN. The eluent from the three elutions was pooled and formic acid (20 μl) was added to lower the pH. The samples were frozen at

−80°C and lyophilized to dryness before liquid chromatography (LC)-MS analysis.

LC-MS/MS analysis

The peptide mixtures were separated by on-line reversed phase chromatography using a Thermo Scientific EASY-nLC II system with a reversed-phase pre-column Magic C-18AQ (100-μm I.D., 2-cm length, 5 μm, 100 Å, Michrom BioResources Inc) pre-column and a reversed phase nano-analytical column Magic C-18AQ (75-μm I.D., 15-cm length, 5 μm, 100 Å, Michrom BioResources Inc) both in-house prepared, at a flow rate of 300 nl/min. The chromatography system was coupled to an LTQ Orbitrap Velos mass spectrometer equipped with a Nanospray II source (ThermoFisher Scientific). Solvents were A: 2% acetonitrile, 0.1% formic acid; B: 90% acetonitrile, 0.1% formic acid. After a 249 bar (~5 μl) pre-column equilibration and 249 bar (~8 μl) nanocolumn equilibration, samples were separated by a 55-min gradient (0 min: 5%B; 45 min: 45%B; 2 min: 80%B; 8 min: 80%B). The LTQ Orbitrap Velos (ThermoFisher Scientific) parameters were as follows: nano-electrospray ion source with spray voltage 2.2 kV, capillary temperature 225°C. Survey MS1 scan *m/z* range 400–2000 profile mode, resolution 60,000 at 400 m/z with AGC target 1E6, and one microscan with maximum inject time 200 ms. Lock mass Siloxane 445.120024 for internal calibration with preview mode for FTMS master scans: on, injection waveforms: on, monoisotopic precursor selection: on; rejection of charge state: 1. The eight most intense ions charge state 2–4 exceeding 5000 counts were selected for CID ion trap MSMS fragmentation (ITMS scans 2–9) and detection in centroid mode. Dynamic exclusion settings were: repeat count: 2; repeat duration: 15 s; exclusion list size: 500; exclusion duration: 60 s with a 10 ppm mass window. The CID activation isolation window was: 2 Da; AGC target: 1E4; maximum inject time: 25 ms; activation time: 10 ms; activation Q: 0.250; and normalized collision energy 35%.

Data analysis parameters

Raw files were analyzed with Proteome Discoverer 1.3.0.339 software suite (Thermo Scientific). Parameters for the Spectrum Selection to generate peak lists of the CID spectra (activation type: CID; s/n cutoff: 1.5; total intensity threshold: 0; minimum peak count: 1; precursor mass: 350–5000 Da) The peak lists were submitted to an in-house Mascot 2.2 against the Uniprot-Swissprot 20110104 (523,151 sequences; 184,678,199 residues) Allspecies taxonomy and Mouse only database as follows: precursor tolerance 8 ppm; MS/MS tolerance 0.6 Da; Trypsin enzyme 1 missed cleavages; FT-ICR ESI instrument type; fixed modification: carbamidomethylation (C); variable modifications: deamidation (N, Q); oxidation (M), propionamide (C), and phosphorylated (T, Y, S). Percolator settings: max δ Cn 0.05; target FDR strict 0.01, target FDR relaxed 0.05 with validation based on *q* value.

Additional searches were performed against IPI_mouse 3_47 (110 771 sequences; 49,890,456 residues).

In vitro phosphorylation assay

An *in vitro* phosphorylation assay was designed to assess the role of phosphorylation on S402. In this radiometric assay, three different proline directed kinases, cyclin-dependent kinase 2 (CDK2), extracellular signal-regulated kinase 2 (ERK2), and GSK3β, were tested for their ability to phosphorylate the S402 residue on KIF1A by the Kinexus substrate profiling services (Vancouver, BC). The various recombinant protein kinases employed in the substrate profiling process were cloned, expressed and purified using proprietary methods. Quality control testing is routinely performed on each of the kinases to ensure compliance to acceptable standards. The [γ-^{33}P] ATP was purchased from PerkinElmer. All other materials were of standard laboratory grade. A total of 2 mg of each peptide was synthesized based on a peptide sequence of interest as listed below:

1. KSP04-CAF KIF1A [S402] WT KKALVGMSPSS-pS-L >98%
2. KSP04-CBT KIF1A [A402] mutant (MT) KKALVGMAPSS-pS-L >98%.

Inducible Golgi dispersion assay

The rat KIF1A(FL)-V483N coding sequence (Soppina et al., 2014) was tagged with monomeric NeonGreen and an FRB domain. Mutations of S411E and S411A were introduced by QuikChange mutagenesis. Plasmids for expression of WT or mutant motors were cotransfected into COS-7 cells with a plasmid for expression of GMAP210-mRFP-2xFKBP at a ratio of 6:1 with TransIT-LT1 transfection reagent (Mirus). Sixteen hours after transfection, rapamycin (Calbiochem, Millipore Sigma) was added to a final concentration of 44 nM to promote FRB and FKBP heterodimerization and recruitment of motors to the Golgi. After 30 min, the cells were fixed with 3.7% formaldehyde (ThermoFisher Scientific) in 1× PBS for 10 min, quenched in 50 mM ammonium chloride in PBS for 5 min, permeabilized with 0.2% Triton X-100 in PBS for 10 min, and then incubated in blocking buffer (0.2% fish skin gelatin in PBS). Primary [polyclonal antibody against *cis*-Golgi marker giantin (1:1200 PRB-114C, Covance)] and secondary antibodies [Alexa Fluor 680-labeled goat anti-rabbit (1:500, Jackson ImmunoResearch) and DAPI (final concentration 10.9 μM)] were added to blocking buffer and incubated for 1 h each at room temperature. Coverslips were mounted in ProlongGold (Invitrogen) and imaged using an inverted epifluorescence microscope (Nikon TE2000E) with a 40 × 0.75 NA objective and a CoolSnapHQ camera (Photometrics).

Golgi localization before and after motor recruitment was quantified using a distance-based analysis using a custom ImageJ plugin (Budaitis et al., 2019) for $N \geq 26$ cells across two independent experiments. Briefly, (1) a custom ImageJ plugin generates a line scan from the centroid of the nucleus to the periphery of the cell; this is repeated every one degree for a total of 360 linescans around the cell. The fluorescence intensity along each line scan is determined. (2) For background subtraction, a line scan starting from the centroid of the nucleus to the cell periphery is generated in a region of the cell that lacks cargo and is subtracted from each line scan (scaled background subtraction). Distances that correspond to regions inside the nucleus are removed from each line scan, such that point 0 corresponds to the edge of the nuclear membrane. Oversampling of pixels in the center of the cell was corrected, following the assumption that the cell is a perfect circle. (3) The total distance of each line scan was normalized to itself, such that the distance of each line scan was between 0 (nuclear membrane) and 1 (cell periphery). (4) Pixel intensities were grouped in bins by distance (width, 0.05) and only the top 200 pixels within each bin were included in further analysis. (5) Pixel intensity was averaged for each binned distance to generate a dispersion profile for the cell.

Statistical analyses

Statistical analyses were performed using Microsoft Excel or GraphPad Prism. For KIF1A live imaging experiments in hippocampal neurons, motor protein flux is presented as mean ± SEM. All experiments were performed on at least 15 cells from three independent cultures. All statistical analyses were performed using one-way ANOVAs with Tukey's *post hoc* tests, comparing control and treated conditions within the same experiments. For inducible Golgi dispersion assays, the fluorescence intensity for each normalized distance bin was averaged across all cells in two independent experiments and the data were plotted as mean ± SEM. The statistical differences in mean fluorescence intensity were calculated at each binned distance comparing the WT and MT motor for each condition (–Rap and +Rap) using a two-tailed unpaired Student's *t* test. Differences between the WT and MT motors at $p < 0.05$ are indicated by an asterisk. WT – Rap, $n = 26$ cells; WT + Rap, $n = 31$ cells; S411A – Rap, $n = 30$ cells; S411A + Rap, $n = 29$ cells; S411E – Rap, $n = 27$ cells; S411E + Rap, $n = 28$ cells.

Results

AβOs impair KIF1A transport independent of tau

Previously, Ramser et al. (2013) discovered that AβOs disrupt BDNF transport independent of tau hyperphosphorylation, microtubule destabilization, and neuronal toxicity. These findings raised the intriguing possibility that KIF1A, the primary kinesin motor required for BDNF transport (Barkus et al., 2008; Lo et al., 2011; Kondo et al., 2012), is directly impaired in AβO-treated neurons by a mechanism independent of tau. In the present study, we cultured hippocampal neurons from WT (tau$^{+/+}$) and tau knock-out (tau$^{-/-}$) mice, expressed mouse KIF1A tagged with enhanced green fluorescent protein (KIF1A-eGFP) in these neurons at 10 DIV, and added vehicle solution (control) or 500 nM AβOs to their culture medium at 11 DIV (Fig. 1A). Irreversible AβO binding was confirmed retrospectively by immunocytochemistry (Fig. 1B) using an oligomer-selective antibody (NU-4; Lambert et al., 1998). After 18 h of treatment, we imaged KIF1A-eGFP transport and compared the flux, velocity, and run length of axonal KIF1A puncta across all conditions (Fig. 1C; Table 1).

A   Timeline of Imaging Experiments
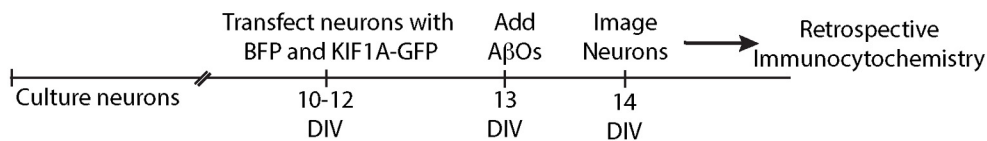
B   Expression of KIF1A-GFP in an AβO treated neuron
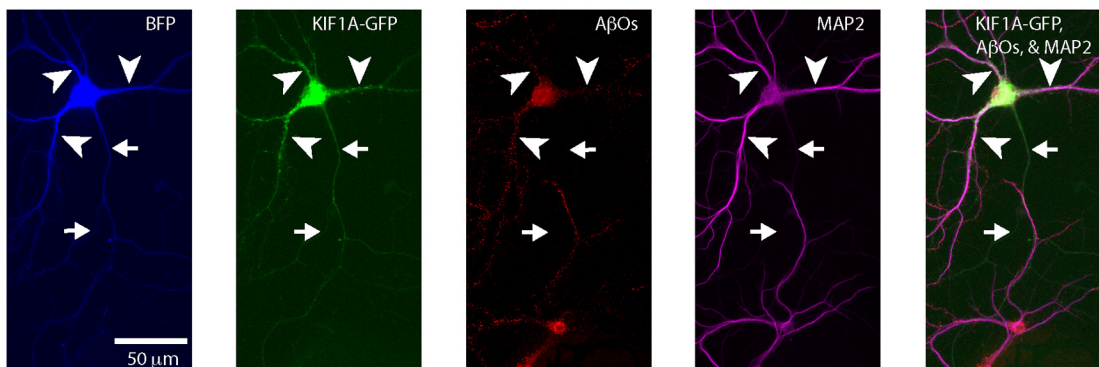
C   Chemical Inhibition of GSK3β prevents AβO-induced transport defects
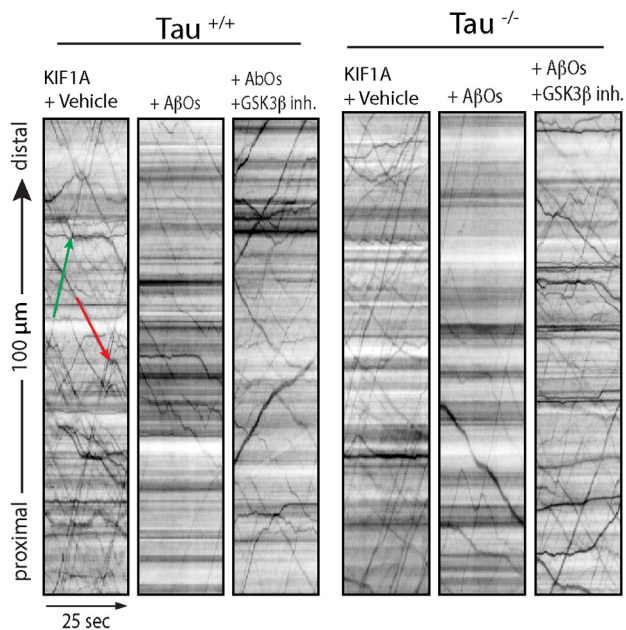
D   KIF1A transport in Tau $^{+/+}$ neurons
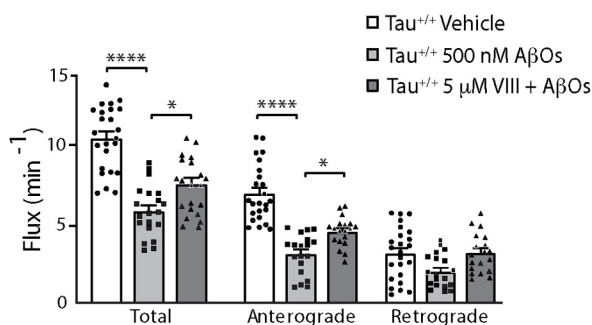
E   KIF1A transport in Tau $^{-/-}$ neurons
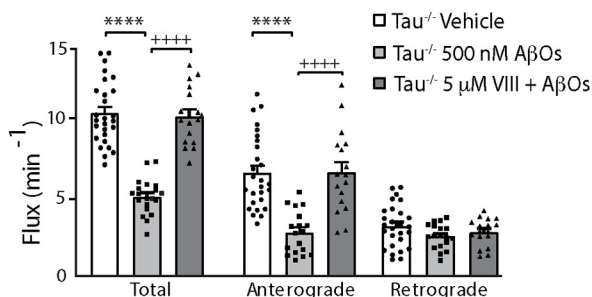
Figure 1. AβO treatment blocks KIF1A transport in a GSK3β-dependent and tau-independent manner. **A**, Schematic of the timeline of experiments. **B**, Representative image of soluble BFP and KIF1A-eGFP expressed in an AβO-treated tau$^{+/+}$ neuron. AβOs binds exclusively to dendrites and remain oligomeric after 18 h in culture. Arrows indicate axon; arrowheads indicate dendrites. **C**, Effects of AβOs and Inhibitor VIII treatment on KIF1A-GFP flux in tau$^{+/+}$ and tau$^{-/-}$ neurons. Representative kymographs comparing KIF1A-GFP transport in control and treated neurons. Lines with a positive slope represent anterograde transport (green); lines with a negative slope represent retrograde transport (red). **D, E**, Vesicle flux is significantly reduced in tau$^{+/+}$ and tau$^{-/-}$ AβO-treated neurons and is restored by treatment with GSK3β Inhibitor VIII. All bar graphs display mean ± SEM; at least 15 cells from three independent cultures were analyzed. Statistical significance was evaluated by one-way ANOVA with Tukey's *post hoc*

continued

comparisons; $*p < 0.05$ and $****p < 0.0001$ when compared with vehicle; $+p < 0.05$ and $++++p < 0.0001$ when compared with AβOs; nonsignificant relations are not indicated. For complete transport statistics, see Table 1 and Extended Data Table 1-1.

Representative kymographs illustrate differences between KIF1A transport in control and AβO-treated neurons (Fig. 1C). AβO treatment dramatically reduced anterograde KIF1A flux in both tau$^{+/+}$ and tau$^{-/-}$ neurons, indicating that tau is not required for AβO disruption of KIF1A transport (Fig. 1D,E; Table 1). AβOs also significantly decreased anterograde average velocity and run length in tau$^{-/-}$ neurons. Retrograde movement of KIF1A, presumably driven by cytoplasmic dynein, was also decreased on AβO treatment, although the effect in tau$^{-/-}$ neurons was not statistically significant (Table 1). In all experiments, KIF1A transport parameters were similar to those previously reported for BDNF (Lo et al., 2011; Seifert et al., 2016; Bodakuntla et al., 2020), implying that changes in KIF1A motility are not attributed to overexpression artefacts. These results demonstrate that AβOs reduce KIF1A motility independent of tau.

GSK3β inhibition prevents KIF1A transport defects in AβO-treated neurons

Pharmacological inhibition and dominant negative mutations of GSK3β prevent BDNF transport defects induced by AβOs (Ramser et al., 2013). This effect is observed in both tau$^{+/+}$ and tau$^{-/-}$ neurons, ruling out the possibility that tau activates PP1-GSK3β signaling to block transport, as reported previously for KIF5 in isolated squid axoplasm (Kanaan et al., 2011). Does GSK3β impair transport by reducing KIF1A motility in AβO-treated neurons, and does GSK3β require tau for this function? We incubated tau$^{+/+}$ and tau$^{-/-}$ neurons with 5 μM Inhibitor VIII (a selective, cell-permeable, competitive blocker of GSK3β; Bhat et al., 2003) for 30 min before AβO treatment. Pretreatment with Inhibitor VIII prevented defects in KIF1A flux, velocity and run length (Fig. 1C–E; Table 1). Thus, consistent with previous findings for BDNF transport (Ramser et al., 2013), GSK3β mediates KIF1A transport impairment in AβO-treated neurons. This observed effect was comparable in both tau$^{+/+}$ and tau$^{-/-}$ neurons (Fig. 1B; Table 1), demonstrating that GSK3β reduces KIF1A motility independent of tau.

KIF1A interacts with GSK3β and is phosphorylated at a conserved GSK3β consensus site

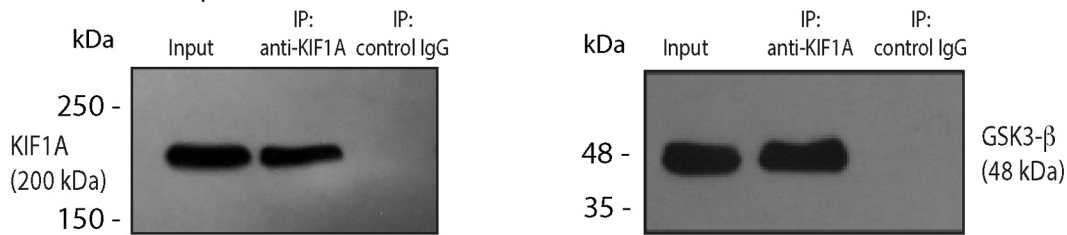GSK3β has been shown to associate with kinesin-1 motor complexes (Morfini et al., 2002). To determine whether KIF1A interacts with GSK3β, we generated cell lysates from mouse hippocampi and immunoprecipitated KIF1A using a specific monoclonal antibody (Fig. 2A). By immunoblotting, we found that GSK3β coimmunoprecipitates with input and KIF1A proteins, but not with negative control IgG proteins alone (Fig. 2A). This result indicates that KIF1A and GSK3β interact, either by forming a direct complex or by binding indirectly through scaffold proteins.

To identify specific residues of KIF1A that are phosphorylated by GSK3β, we isolated KIF1A from 14-month-old WT and Tg2576 (APP$_{Swe}$) mouse brains by immunoprecipitation and resolved the proteins by SDS-PAGE. Following in-gel tryptic digestion, the resulting peptides were analyzed by sequential LC-MS/MS. Although immunoblots with pan-phospho-Ser and pan-phospho-Thr antibodies failed to detect any phospho-KIF1A immunoreactivity (Extended Data Fig. 1-1), we detected nine phosphopeptides in KIF1A (UniProtKB/Swiss-Prot: Q6TA13), four of which conform to sequences targeted by kinases that are aberrantly activated in AD including mitogen-activated protein kinase (MAPK), casein kinase II (CK2), and GSK3β (Fig. 2B,C; Extended Data Fig. 2-1; Maqbool et al., 2016; Cline et al., 2018). Because our analyses were not quantitative, we were unable to establish whether these phospho-sites were more abundant in Tg2576 mice relative to WT mice. We compared high confidence KIF1A phosphopeptides in WT and Tg2576 mice using PhosphoRS and mapped them to specific sites within KIF1A functional domains (Fig. 2B). Phosphorylation within specific KIF1A sequences varied between genotypes; for example, S937, located within the presumed cargo-binding peptide SGTS*QEELR, was phosphorylated (denoted by *) in Tg2576 mice but not detected in WT mice (Fig. 2D). However, S937 did not conform to an AD-related kinase motif according to the Phosida and Phosphonet databases. Based on these analyses, we focused on S402 (Fig. 2D) as it (1) is located between the neck-coil domain and the first coiled-coil domain and could therefore impact motor dimerization and/or motility (Fig. 2B; Al-Bassam et al., 2003; Hammond et al., 2009; Soppina et al., 2014), (2) conforms to a GSK3β consensus site, and (3) is conserved between zebrafish, mouse, rat, and human KIF1A proteins (Fig. 2E).

GSK3β phosphorylates KIF1A at S402 *in vitro*

To confirm phosphorylation of S402 and evaluate whether GSK3β can perform this modification, we developed a sensitive *in vitro* radiometric enzyme assay (Fig. 2F). We synthesized a WT KIF1A peptide containing S402 and a phosphomutant KIF1A peptide containing an alanine substitution at S402 (S402A). We then tested three different proline-directed kinases (CDK2, ERK2, and GSK3β) for their ability to phosphorylate these peptides. Mutation of S402 nearly abolished the ability of GSK3β to phosphorylate the S402-containing peptide whereas the kinase activities of CDK2 and ERK2 were less impacted by the S402A mutation (Fig. 2F). These results confirm that S402 is phosphorylated by GSK3β *in vitro* and support a plausible role for this residue in regulating KIF1A motility.

A   KIF1A binds GSK3β in cultured neurons

kDa	Input	IP: anti-KIF1A	IP: control IgG

KIF1A
(200 kDa)

250 -

150 -

kDa	Input	IP: anti-KIF1A	IP: control IgG

GSK3-β
(48 kDa)

48 -

35 -

B   Schematic of the domain organization of KIF1A

Liprin-α binding
domain
657-1105

Motor domain	Neck-coil	Coiled coil 1	FHA domain	Coiled coil 2	Coiled coil 3	PH domain

NH2 — COOH

amino acids 1-361   365-397   429-462   516-572   622-681   801-822   1676-1774
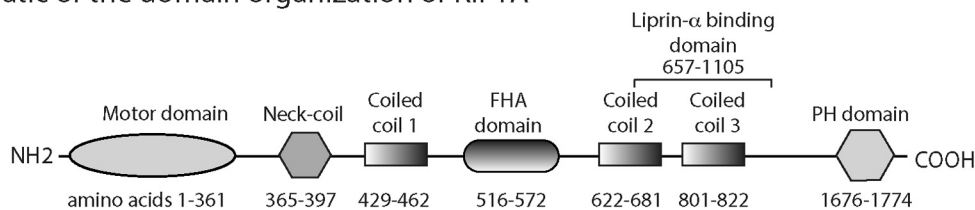
C   Identification of phosphorylated peptides in KIF1A by mass spectrometry

Sequence	MH+ [Da]	Mascot Score WT/AD	Expected value WT/AD	Predicted Kinase
394-MTNALVGMS*PSSSL-406	2058.0	79/65	$1.9 \times 10^{-6}/4.8 \times 10^{-5}$	GSK3β
934-SGTS*QEELR-942	1086.4	N.A/31	N.A./0.045	Casein kinase II
1326-VTGVYELSLCHVADAGS*PGMQR-1347	2444.1	63/45	0.0001/0.008	ERK/MAPK
1535-PAS*PEPELLPELDSK-1546	1701.8	37/32	0.03/0.089	GSK3β

D   Identification of S402 phosphopeptide

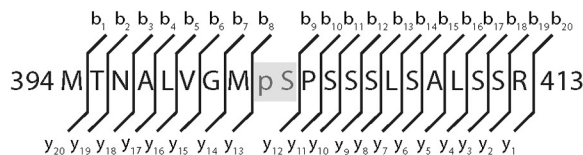b_1 b_2 b_3 b_4 b_5 b_6 b_7 b_8 b_9 b_{10} b_{11} b_{12} b_{13} b_{14} b_{15} b_{16} b_{17} b_{18} b_{19} b_{20}

394 M T N A L V G M pS P S S S L S A L S S R 413

y_{20} y_{19} y_{18} y_{17} y_{16} y_{15} y_{14} y_{13} y_{12} y_{11} y_{10} y_9 y_8 y_7 y_6 y_5 y_4 y_3 y_2 y_1

E   Conservation of GSK3β consensus sequence

Mus	394	MTNALVGMSPSSSLSALSSR 413
Rattus	403	MTNALVGMSPSSSLSALSSR 422
Danio	431	- TNAMTGMSPSPSLSALSSR 449
Homo	394	MTNALVGMSPSSSLSALSSR 413

F   *In vitro* phosphorylation of the KIF1A MTNALVGMSPSSSL peptide

Protein Kinase	KIF1A S402 WT peptide (counts/min)	KIF1A S402A MT peptide (counts/min)	Difference (MT-WT)/WT	% Change
GSK3β	51,748	1,512	50,237	-97%
CDK2	5,556	2,440	3,116	-56%
ERK2	2,631	1,957	674	-26%

Figure 2. GSK3β phosphorylates KIF1A at several sites. ***A***, A monoclonal antibody to KIF1A immunoprecipitated GSK3β from neuronal lysates. ***B***, Schematic of the domain organization of KIF1A (GenBank BAA0622.1). ***C***, Tandem mass spectroscopy on KIF1A isolated from WT and AD model mouse (APPswe; AD) brain identified four phosphopeptides which conform to sites targeted by kinases that are aberrantly activated in AD, such as MAPK, CK2, and GSK3β. Serine 402 conforms to a GSK3β phosphorylation site according to Phosida (http://141.61.102.18/phosida/index.aspx) and Phosphonet (https://kinexus.ca). ***D***, MS identification of the *b*+ and *y*+ ions that are the direct (N to C terminus) and reverse (C to N terminus) ion series obtained during collision-induced dissociation (also see Extended Data Fig. 1-1). ***E***, Sequence comparison of the region surrounding Serine 402 between zebrafish, mouse,

continued

rat, and human proteins. **F**, The evaluation of three different proline-directed kinases (CDK2, ERK2, and GSK3β) by radiometric assay indicates that GSK3β shows a strong preference for the KIF1A (S402) WT peptide over the A402 MT peptide *in vitro*.

Point mutations of S402 do not alter KIF1A motility

Does phosphorylation at S402 regulate KIF1A motility? We generated a non-phosphorylatable form of KIF1A-eGFP by inducing a Ser-to-Ala point mutation (KIF1A-S402A) at this site. Conversely, we induced a Ser-to-Glu point mutation to mimic GSK3β phosphorylation of KIF1A-eGFP at this site (KIF1A-S402E). We expressed these mutants in mouse hippocampal neurons and compared their motility to WT KIF1A by live cell imaging (Fig. 3A). Representative kymographs and quantification of transport parameters revealed no significant differences in flux, run length and velocity for KIF1A-S402A or KIF1A-S402E relative to WT KIF1A (Fig. 3A; Table 2; Extended Data Table 1-1). These data imply that S402 phosphorylation does not regulate KIF1A transport in hippocampal neurons. We next asked whether AβO-induced overactivation of GSK3β impairs KIF1A transport via phosphorylation at S402. We compared the motility of WT KIF1A-eGFP and KIF1A-S402A-eGFP in control and AβO-treated neurons (Fig. 3B; Table 2; Extended Data

Table 1-1). Kymograph analyses revealed that AβO treatment similarly reduced the anterograde fluxes, velocities and run lengths of the WT and mutant motors, indicating that the alanine point mutation does not protect against KIF1A transport defects. Taken together, these results indicate that GSK3β does not regulate KIF1A motility through phosphorylation at S402A.

As an alternative explanation for this outcome, endogenous WT KIF1A may dimerize with mutant KIF1A monomers or preferentially bind to cargo, thus masking any effects of the mutations on KIF1A motility. To investigate the effects of S402A and S402E point mutations on KIF1A motility in the absence of endogenous KIF1A transport, we performed an inducible Golgi dispersion assay in COS7 cells (Engelke et al., 2016; Budaitis et al., 2019; Fig. 4A; Extended Data Figs. 4-1, 4-2). In this assay, Golgi-targeted kinesin motors cause the dispersion of the Golgi complex from its characteristic tightly-packed, perinuclear location to a phenotype consisting of small Golgi-derived vesicles scattered throughout the cytoplasm

Table 1: Quantitative analysis of axonal KIF1A-GFP transport in tau$^{+/+}$ and tau$^{-/-}$ neurons.

		Traffic values	
	All Events	Anterograde	Retrograde
Flux (min–1)			
tau$^{+/+}$ vehicle	10.46 ± 0.48	7.03 ± 0.78	3.35 ± 0.38
tau$^{+/+}$ AβOs	5.83 ± 0.24****	2.71 ± 0.65****	3.12 ± 0.35
tau$^{+/+}$ VII + AβOs	7.56 ± 0.53*#	4.19 ± 0.35#	3.37 ± 0.40
tau$^{-/-}$ vehicle	10.74 ± 0.70	7.38 ± 0.35	3.35 ± 0.33
tau$^{-/-}$ AβOs	5.77 ± 0.43****	3.11 ± 0.25****	2.66 ± 0.32
tau$^{-/-}$ VII + AβOs	10.38 ± 1.01####	7.42 ± 0.76####	2.95 ± 0.38
Velocity (µm/s)			
tau$^{+/+}$ vehicle	1.68 ± 0.12	2.04 ± 0.16	1.33 ± 0.12
tau$^{+/+}$ AβOs	1.63 ± 0.12	1.72 ± 0.17	1.31 ± 0.16
tau$^{+/+}$ VII + AβOs	1.75 ± 0.08	1.48 ± 0.18	1.47 ± 0.09
tau$^{-/-}$ vehicle	1.93 ± 0.07	2.28 ± 0.14	1.55 ± 0.07
tau$^{-/-}$ AβOs	1.41 ± 0.18*	1.54 ± 0.19*	1.30 ± 0.19
tau$^{-/-}$ VII + AβOs	1.98 ± 0.11#	2.35 ± 0.16#	1.54 ± 0.12
Run length (µm)			
tau$^{+/+}$ vehicle	18.85 ± 1.09	26.02 ± 2.02	12.09 ± 1.30
tau$^{+/+}$ AβOs	17.26 ± 1.65	19.74 ± 2.83	13.37 ± 2.00
tau$^{+/+}$ VII + AβOs	17.48 ± 0.94	23.05 ± 1.67	10.96 ± 0.76
tau$^{-/-}$ vehicle	20.39 ± 1.05	27.32 ± 2.13	13.75 ± 1.21
tau$^{-/-}$ AβOs	11.27 ± 0.88****	13.38 ± 1.11***	9.82 ± 0.91
tau$^{-/-}$ VII + AβOs	20.79 ± 2.01####	29.38 ± 3.77###	12.64 ± 0.72

tau$^{+/+}$ vehicle: n = 24 kymographs (24 cells, 893 puncta).
tau$^{-/-}$ vehicle: n = 27 kymographs (27 cells, 1014 puncta).
tau$^{+/+}$ AβO: n = 18 kymographs (19 cells, 432 puncta).
tau$^{-/-}$ AβO: n = 18 kymographs (18 cells, 578 puncta).
tau$^{+/+}$ VIII + AβO: n = 18 kymographs (18 cells, 643 puncta).
tau$^{-/-}$ VIII + AβO: n = 17 kymographs (17 cells, 638 puncta).
*$p < 0.05$, when compared with vehicle.
**$p < 0.01$, when compared with vehicle.
***$p < 0.001$, when compared with vehicle.
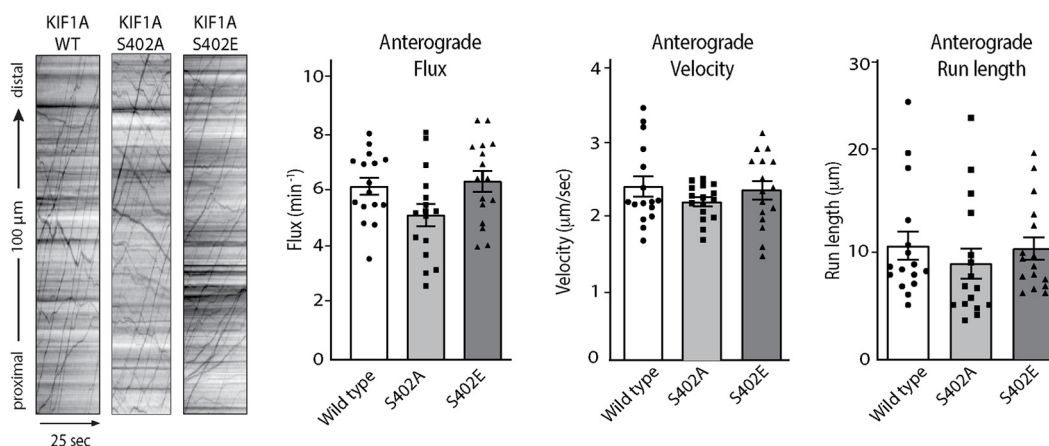****$p < 0.0001$, when compared with vehicle.
#$p < 0.05$, when compared with AβOs.
##$p < 0.01$, when compared with AβOs.
###$p < 0.001$, when compared with AβOs.
####$p < 0.0001$, when compared with AβOs.

A Phosphomutants of S402 do not influence KIF1A anterograde motility in neurons

B The phosphomutant S402A does not prevent KIF1A anterograde motility defects in AβO-treated neurons
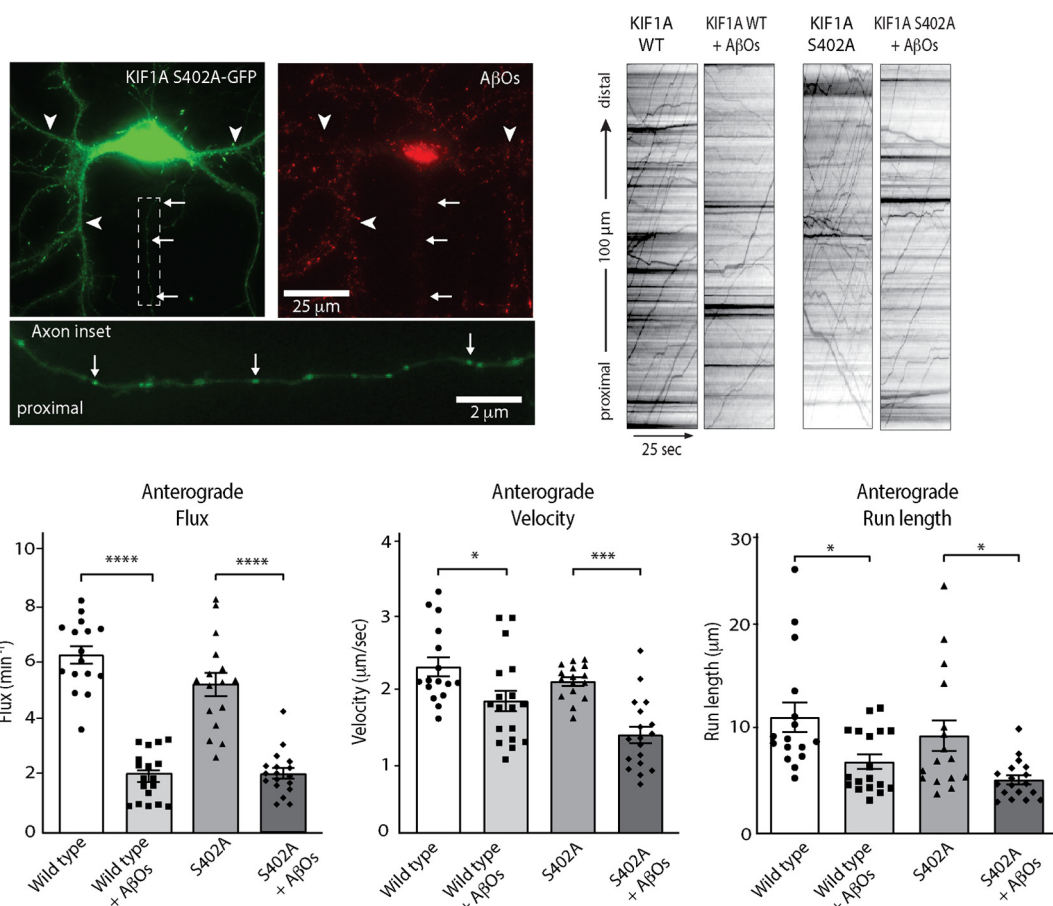

Figure 3. Phospho-mutants of Serine402 do not alter KIF1A-mediated transport. **A**, Representative kymographs comparing KIF1A-eGFP WT, S402A, and S402E transport in WT neurons. Bar graphs display mean ± SEM; at least 15 cells from three independent cultures were analyzed. Statistical significance was evaluated by one-way ANOVA with Tukey's *post hoc* comparisons; nonsignificant relations are not indicated. For complete statistics, see Table 2 and Extended Data Table 1-1. **B**, Representative image of KIF1A S402A-eGFP expressed in an AβO-treated WT neuron. AβOs bind exclusively to dendrites and remain oligomeric after 18 h in culture. Arrows indicate axon; arrowheads indicate dendrites. Representative kymographs comparing KIF1A-eGFP WT and S402A transport in control and AβO-treated neurons. Bar graphs display mean ± SEM; at least 15 cells from three independent cultures were analyzed. Statistical significance ($*p < 0.05$, $**p < 0.01$, $*** p < 0.001$, $****p < 0.0001$) was evaluated by one-way ANOVA with Tukey's *post hoc* comparisons; nonsignificant relations are not indicated. For complete statistics, see Table 2 and Extended Data Table 1-1.

Table 2: Quantitative analysis of axonal KIF1A-S402A and KIF1A-S402E transport in tau$^{+/+}$ neurons

		Traffic values	
	All events	Anterograde	Retrograde
Flux (min^{-1})			
WT	8.00 ± 0.46	6.11 ± 0.30	1.88 ± 0.30
WT + ABO	$3.05 \pm 0.46^{****\#\#\#\#}$	$1.94 \pm 0.20^{****\#\#\#\#}$	$1.12 \pm 0.20^{\#\#\#\#}$
S402A	7.72 ± 0.34	5.10 ± 0.40	2.71 ± 0.27
S402A + ABO	$3.80 \pm 0.24^{****\#\#\#\#}$	$2.04 \pm 0.18^{****\#\#\#\#}$	$2.71 \pm 0.27^{\#}$
S402E	7.63 ± 0.42	6.30 ± 0.37	$1.34 \pm 0.17^{\#\#}$
Velocity (μm/s)			
WT	2.05 ± 0.11	2.28 ± 0.13	1.53 ± 0.14
WT + ABO	1.72 ± 0.14	$1.81 \pm 0.14^{*}$	1.55 ± 0.15
S402A	2.03 ± 0.07	2.08 ± 0.06	1.96 ± 0.15
S402A + ABO	$1.23 \pm 0.10^{****\#\#\#\#\$\$}$	$1.35 \pm 0.12^{****\#\#\#\$}$	$1.13 \pm 0.11^{\#\#\#}$
S402E	2.03 ± 0.10	2.23 ± 0.12	1.51 ± 0.12
Run length (μm)			
WT	9.14 ± 1.02	10.74 ± 1.36	5.64 ± 0.57
WT + ABO	$6.26 \pm 0.62^{*}$	$6.62 \pm 0.68^{*}$	5.64 ± 0.89
S402A	7.34 ± 0.90	9.03 ± 1.42	5.31 ± 0.39
S402A + ABO	$4.77 \pm 0.29^{***}$	$4.93 \pm 0.42^{***\#}$	4.53 ± 0.25
S402E	9.09 ± 0.90	10.46 ± 1.08	5.31 ± 0.54

WT: $n = 16$ kymographs (16 cells, 789 puncta).
S402A: $n = 16$ kymographs (16 cells, 829 puncta).
WT + ABO: $n = 18$ kymographs (18 cells, 381 puncta).
S402A + ABO: $n = 18$ kymographs (18 cells, 430 puncta).
S402E: $n = 16$ kymographs (16 cells, 743 puncta).
$^{*}p < 0.05$, when compared with WT.
$^{**}p < 0.01$, when compared with WT.
$^{***}p < 0.001$, when compared with WT.
$^{****}p < 0.0001$, when compared with WT.
$^{\#}p < 0.05$, when compared with S402A.
$^{\#\#}p < 0.01$, when compared with S402A.
$^{\#\#\#}p < 0.001$, when compared with S402A.
$^{\#\#\#\#}p < 0.0001$, when compared with S402A.
$^{\$}p < 0.05$, when comparing A$\beta$O-treated conditions (significance denoted in S402 + AβO condition).
$^{\$\$}p < 0.01$, when comparing A$\beta$O-treated conditions (significance denoted in S402 + AβO condition).
$^{\$\$\$}p < 0.001$, when comparing A$\beta$O-treated conditions (significance denoted in S402 + AβO condition).
$^{\$\$\$\$}p < 0.0001$, when comparing A$\beta$O-treated conditions (significance denoted in S402 + AβO condition).

(Engelke et al., 2016). We used the rapamycin-induced dimerization of FRB and FKBP to drive the rapid recruitment of KIF1A motors to the Golgi surface and determined the effect on Golgi dispersion after 30 min of motor activity. This assay probes the ability of motors to drive transport in a cellular environment and requires motors capable of not only processive motility, but also sufficient force generation to oppose the Golgi-localized dynein that is responsible for the perinuclear clustering of this organelle (Corthésy-Theulaz et al., 1992; Burkhardt et al., 1997).

Because full-length KIF1A resides in an inactive, autoinhibited state, we first introduced a point mutation (V483N) that relieves the self-inhibition of motor activity (Huo et al., 2012; Yue et al., 2013; Soppina et al., 2014). Using this active version of full-length KIF1A, we then introduced point mutations that could abolish or mimic the phosphorylation state of the S402 residue. Using the rat KIF1A sequence, these mutations are S411A and S411E, respectively. WT and MT full-length KIF1A(V483N) motors were fused to mNeonGreen and a FRB domain, whereas the Golgi targeting sequence of the *cis*-Golgi resident protein GMAP210 was fused to monomeric red fluorescent protein (mRFP) and the FKBP domain (Engelke et al., 2016). Addition of rapamycin resulted in rapid recruitment of WT, S411A, and S411E motors to the Golgi surface and subsequent transport of Golgi particles to the cell

periphery. No differences in Golgi dispersion were observed between the WT, S411A and S411E motors (Fig. 4A; Extended Data Fig. 4-2). These results indicate that the phosphorylation state of S411 does not impact the motility and force generation of KIF1A in this system. Alternatively, it is possible that the Ser-to-Glu mutation does not mimic KIF1A phosphorylation in this context (Dephoure et al., 2013).

Discussion

Impairment of axonal transport is an early pathologic event that leads to axonal degeneration and loss of synapse function in AD (Stokin et al., 2005; Minoshima and Cross, 2008; Gallagher et al., 2012; Sleigh et al., 2019). Soluble AβOs, a causative agent of AD (Cline et al., 2018), activate intracellular signaling cascades that trigger aberrant phosphorylation of many target proteins, including tau. Many studies have examined how tau hyperphosphorylation, microtubule destabilization, and cytoskeletal collapse impair transport (Mandelkow et al., 2003; Stokin and Goldstein, 2006; Cowan et al., 2010; Combs et al., 2019). However, subtler mechanisms of AβO-induced transport disruption that arise before neurotoxicity and that act directly on motor proteins to reduce their motility have received much less attention and have not been investigated in mammalian neurons.
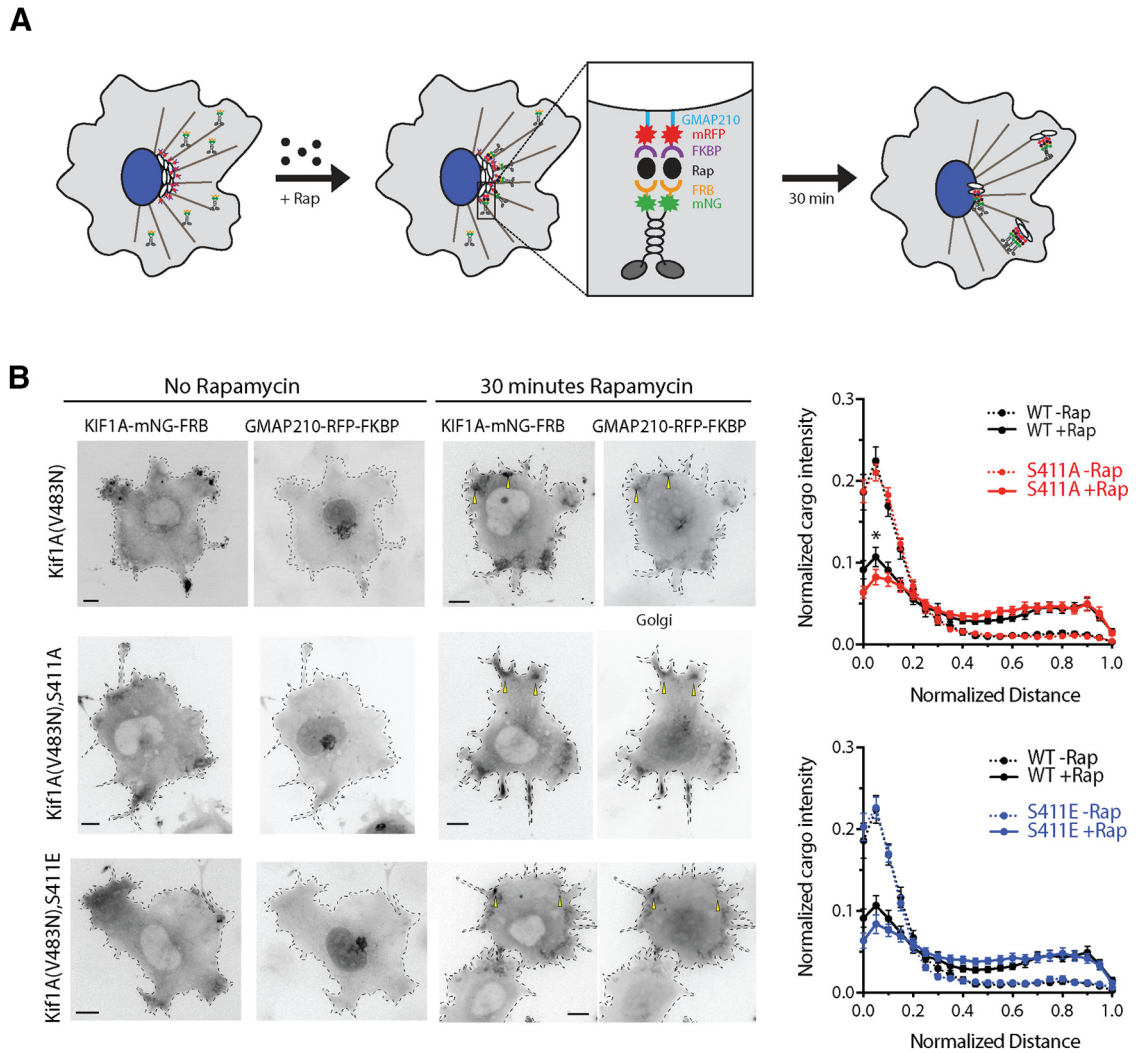
Figure 4. A phospho-mutant of S402 does not influence KIF1A activity in Golgi-dispersion assays. **A**, Schematic of the inducible motor recruitment assay. A kinesin motor tagged with monomeric NeonGreen (mNG) and an FRB domain (KIF1A-mNG-FRB) is coexpressed with a Golgi targeting sequence (GMAP210) tagged with mRFP and FKBP domain (GMAP210-mRFP-FKBP) in COS7 cells. Addition of rapamycin (+Rap) causes heterodimerization of the FRB and FKBP domains and recruitment of motors to the cargo membrane. Recruitment of active motors drives cargo dispersion to the cell periphery. **B**, COS7 cells expressing WT, S411A, or S411E versions of full-length active (V483N) KIF1A-mNG-FRB together with GMAP210-mRFP-2xFKBP were treated with ethanol vehicle (no rapamycin, left panels) or with 44 nM rapamycin (middle panels). After 30 min, the cells were fixed and stained with an antibody to the Golgi marker giantin (data not shown) and DAPI (data not shown). Representative images of the KIF1A-mNG-FRB (KIF1A motor) and GMAP210-mRFP-2xFKBP (Golgi marker) channels are shown in inverse grayscale. Yellow arrowheads indicated examples of dispersed Golgi particles. Scale bars: 10 μm. The Golgi distribution in the giantin channel was quantified and the data are displayed as the fluorescence intensity of Golgi particles on the *y*-axis and the normalized distance on the *x*-axis (0.0 = edge of nucleus, 1.0 = plasma membrane). WT −Rap (dotted black lines), $n = 26$ cells; WT +Rap (solid black lines), $n = 31$ cells; S411A −Rap (dotted red line), $n = 30$ cells; S411A +Rap (solid red line), $n = 29$ cells; S411E −Rap (dotted blue line), $n = 27$ cells; S411E +Rap (solid blue line), $n = 28$ cells across two independent experiments. Statistical differences in mean cargo intensity between WT and MT motors were calculated at each binned distance and for each condition (−Rap and +Rap) by using a two-tailed unpaired Student's *t* test; $* p < 0.05$. For complete statistical analysis, see Extended Data Figure 4-2.

Here, through direct assessment of trafficking at high spatial and temporal resolution in mouse hippocampal neurons, we demonstrate that AβOs impair KIF1A motility independent of tau (Fig. 1). These results are consistent with previous findings that AβOs impair motility of the KIF1A cargo protein BDNF and that this defect is independent of tau (Ramser et al., 2013). We also demonstrate that pharmacological inhibition of GSK3β prevented

these transport defects (Fig. 1), motivating us to investigate whether KIF1A motility is dysregulated by phosphorylation. By MS, we identified nine phosphorylation sites on KIF1A, four of which are targeted by kinases associated with AD, including GSK3β (Fig. 2). We discovered that S402, located proximal to the neck-coil domain of KIF1A, conforms to a highly conserved GSK3β consensus site (Fig. 2). Using an *in vitro* kinase assay, we

confirmed that S402 is indeed phosphorylated by GSK3β (Fig. 2). Finally, we tested whether a phosphomimic of S402 could modulate KIF1A motility in cultured neurons and in a Golgi dispersion assay using COS-7 cells that lacked endogenous KIF1A. Unfortunately, in both experimental systems, no significant differences in transport properties were observed between WT and mutant KIF1A (Figs. 3 and 4). From these findings, we conclude that GSK3β impairs KIF1A transport independent of tau but likely does not achieve this effect by phosphorylating KIF1A at S402.

Traditionally, axonal transport defects were viewed as a consequence of tau hyperphosphorylation and aggregation, tau-induced kinase activation, microtubule dissolution, and axonal dystrophy during the advanced stages of disease progression (Mandelkow et al., 2003; Stokin and Goldstein, 2006; LaPointe et al., 2009; Morfini et al., 2009; Kanaan et al., 2011). However, transport defects can occur independent of tau and before overt morphologic decline and cell death, suggesting that early transport defects might play a causal role in AD pathogenesis (Pigino et al., 2003; Lazarov et al., 2007; Stokin et al., 2008; Goldstein, 2012; Rodrigues et al., 2012; Ramser et al., 2013). Recent reports indicate that overactivation of GSK3β contributes to many pathologic hallmarks of AD including increased Aβ production, tau hyperphosphorylation, and impaired learning and memory (Maqbool et al., 2016). Data from our present study suggest, pending identification of the specific phosphorylation sites, that the pathologic activation of GSK3β can impair transport by earlier, subtler mechanisms that involve inhibitory phosphorylation of motor proteins. Such mechanisms of GSK3β-dependent motor protein inhibition have been characterized previously in invertebrate models of AD. As a negative regulator of axonal transport in *Drosophila*, active GSK3β binds and phosphorylates kinesin-1 and reduces the number of motors bound to microtubules (Weaver et al., 2013; Banerjee et al., 2018). Alternatively, kinesin motor activity can be inhibited by cargo detachment; in isolated squid axoplasm treated with AβOs, GSK3β phosphorylates kinesin light chain-2, promoting motor-cargo dissociation and impairing transport (Morfini et al., 2002). Interestingly, and perhaps paradoxically, we found a significant effect on KIF1A run lengths and velocity in the tau$^{-/-}$ neurons treated with AβOs (Fig. 1; Table 1). AβOs dysregulate a number of intracellular cascades, including those active toward tau (Cline et al., 2018). It is possible that in the absence of a tau-kinase substrate, these kinases (or phosphatases) aberrantly target regulatory sites on KIF1A that govern processivity akin to the phosphorylation of the motor domain on kinesin-1 in *Drosophila* (Weaver et al., 2013; Banerjee et al., 2018) and KIF5C at S176 (DeBerg et al., 2013). Our study is congruent with those reports and, additionally, is first to show that GSK3β impairs KIF1A motility in a mammalian primary culture model of AD (Fig. 1).

From the nine phosphorylation sites on KIF1A revealed by MS (Fig. 2; Extended Data Fig. 1-1), we chose to investigate S402. This phosphopeptide has also been identified by large scale phosphoproteomic analyses in mouse and human brain (Ullah et al., 2016). However, we found that point mutations of S402 do not regulate KIF1A transport in two cell-based assays (Figs. 3 and 4). As these are negative results, it is possible that the S402E mutation does not fully mimic the addition of a phosphate at this site in the WT motor. It is also possible that single amino acid changes meant to prevent or mimic phosphorylation events are insufficient to alter motor behavior. Indeed, another study found that AMP kinase-dependent phosphorylation of kinesin light chain-1 (KLC1) at S517/S520 does not affect motor function (McDonald et al., 2010). However, several reports demonstrate that increased phosphorylation at a single site is sufficient to impair motor protein motility. Phosphorylation of KIF5C at S176 by JNK weakens motor-microtubule interactions and/or reduces force output (DeBerg et al., 2013; Padzik et al., 2016). Cargo binding, which is required to activate motor proteins, is also disrupted by phosphorylation. MAP kinase phosphorylates KLC1 at S460 to reduce binding and trafficking of calsyntenin-1 (Vagnoni et al., 2011). Moreover, S460 phosphorylation is increased in AD, disrupting axonal transport and promoting amyloidogenic processing of the amyloid precursor protein (APP; Mórotz et al., 2019). Therefore, it may be that phosphorylation at multiple sites synergistically impairs motor motility. Future studies on KIF1A could investigate whether GSK3β and/or other kinases phosphorylate different sites within the motor and cargo-binding domains, and whether mechanisms of cargo dissociation and microtubule detachment converge to impair KIF1A motility.

References

Abney JR, Meliza CD, Cutler B, Kingma M, Lochner JE, Scalettar BA (1999) Real-time imaging of the dynamics of secretory granules in growth cones. Biophys J 77:2887–2895.

Al-Bassam J, Cui Y, Klopfenstein D, Carragher BO, Vale RD, Milligan RA (2003) Distinct conformations of the kinesin Unc104 neck regulate a monomer to dimer motor transition. J Cell Biol 163:743–753.

Banerjee R, Rudloff Z, Naylor C, Yu M, Gunawardena S (2018) The presenilin loop region is essential for glycogen synthase kinase 3β (GSK3β) mediated functions on motor proteins during axonal transport. Hum Mol Genet 27:2986–3001.

Barkus RV, Klyachko O, Horiuchi D, Dickson BJ, Saxton WM (2008) Identification of an axonal kinesin-3 motor for fast anterograde vesicle transport that facilitates retrograde transport of neuropeptides. Mol Biol Cell 19:274–283.

Bhat R, Xue Y, Berg S, Hellberg S, Ormö M, Nilsson Y, Radesäter AC, Jerning E, Markgren PO, Borgegård T, Nylöf M, Giménez-Cassina A, Hernández F, Lucas JJ, Díaz-Nido J, Avila J (2003) Structural insights and biological effects of glycogen synthase kinase 3-specific inhibitor AR-A014418. J Biol Chem 278:45937–45945.

Bloom GS (2014) Amyloid-β and tau: the trigger and bullet in Alzheimer disease pathogenesis. JAMA Neurol 71:505–508.

Bodakuntla S, Schnitzler A, Villablanca C, Gonzalez-Billault C, Bieche I, Janke C, Magiera MM (2020) Tubulin polyglutamylation is a general traffic-control mechanism in hippocampal neurons. J Cell Sci 133:jcs241802.

Brady ST, Morfini GA (2017) Regulation of motor proteins, axonal transport deficits and adult-onset neurodegenerative diseases. Neurobiol Dis 105:273–282.

Budaitis BG, Jariwala S, Reinemann DN, Schimert KI, Scarabelli G, Grant BJ, Sept D, Lang MJ, Verhey KJ (2019) Neck linker docking

is critical for Kinesin-1 force generation in cells but at a cost to motor speed and processivity. Elife 8:e44146.

Burkhardt JK, Echeverri CJ, Nilsson T, Vallee RB (1997) Overexpression of the dynamitin (p50) subunit of the dynactin complex disrupts dynein-dependent maintenance of membrane organelle distribution. J Cell Biol 139:469–484.

Cline EN, Bicca MA, Viola KL, Klein WL (2018) The amyloid-β oligomer hypothesis: beginning of the third decade. J Alzheimers Dis 64:S567–S610.

Combs B, Mueller RL, Morfini G, Brady ST, Kanaan NM (2019) Tau and axonal transport misregulation in tauopathies. Adv Exp Med Biol 1184:81–95.

Corthésy-Theulaz I, Pauloin A, Pfeffer SR (1992) Cytoplasmic dynein participates in the centrosomal localization of the Golgi complex. J Cell Biol 118:1333–1345.

Cowan CM, Bossing T, Page A, Shepherd D, Mudher A (2010) Soluble hyper-phosphorylated tau causes microtubule breakdown and functionally compromises normal tau in vivo. Acta Neuropathol 120:593–604.

DeBerg HA, Blehm BH, Sheung J, Thompson AR, Bookwalter CS, Torabi SF, Schroer TA, Berger CL, Lu Y, Trybus KM, Selvin PR (2013) Motor domain phosphorylation modulates kinesin-1 transport. J Biol Chem 288:32612–32621.

Decker H, Lo KY, Unger SM, Ferreira ST, Silverman MA (2010) Amyloid-beta peptide oligomers disrupt axonal transport through an NMDA receptor-dependent mechanism that is mediated by glycogen synthase kinase 3beta in primary cultured hippocampal neurons. J Neurosci 30:9166–9171.

Dephoure N, Gould KL, Gygi SP, Kellogg DR (2013) Mapping and analysis of phosphorylation sites: a quick guide for cell biologists. Mol Biol Cell 24:535–542.

Engelke MF, Winding M, Yue Y, Shastry S, Teloni F, Reddy S, Blasius TL, Soppina P, Hancock WO, Gelfand VI, Verhey KJ (2016) Engineered kinesin motor proteins amenable to small-molecule inhibition. Nat Commun 7:11159.

Ferreira ST, Lourenco MV, Oliveira MM, De Felice FG (2015) Soluble amyloid-beta oligomers as synaptotoxins leading to cognitive impairment in Alzheimer's disease. Front Cell Neurosci 9:191.

Gallagher JJ, Zhang X, Ziomek GJ, Jacobs RE, Bearer EL (2012) Deficits in axonal transport in hippocampal-based circuitry and the visual pathway in APP knock-out animals witnessed by manganese enhanced MRI. Neuroimage 60:1856–1866.

Gan KJ, Silverman MA (2015) Dendritic and axonal mechanisms of Ca2+ elevation impair BDNF transport in Aβ oligomer-treated hippocampal neurons. Mol Biol Cell 26:1058–1071.

Gan KJ, Silverman MA (2016) Imaging organelle transport in primary hippocampal neurons treated with amyloid-β oligomers. Methods Cell Biol 131:425–451.

Gibbs KL, Greensmith L, Schiavo G (2015) Regulation of axonal transport by protein kinases. Trends Biochem Sci 40:597–610.

Goldstein LS (2012) Axonal transport and neurodegenerative disease: can we see the elephant? Prog Neurobiol 99:186–190.

Hammond JW, Cai D, Blasius TL, Li Z, Jiang Y, Jih GT, Meyhofer E, Verhey KJ (2009) Mammalian kinesin-3 motors are dimeric in vivo and move by processive motility upon release of autoinhibition. PLoS Biol 7:e72.

Hung CO, Coleman MP (2016) KIF1A mediates axonal transport of BACE1 and identification of independently moving cargoes in living SCG neurons. Traffic 17:1155–1167.

Huo L, Yue Y, Ren J, Yu J, Liu J, Yu Y, Ye F, Xu T, Zhang M, Feng W (2012) The CC1-FHA tandem as a central hub for controlling the dimerization and activation of kinesin-3 KIF1A. Structure 20:1550–1561.

Kaech S, Banker G (2006) Culturing hippocampal neurons. Nat Protoc 1:2406–2415.

Kanaan NM, Morfini GA, LaPointe NE, Pigino GF, Patterson KR, Song Y, Andreadis A, Fu Y, Brady ST, Binder LI (2011) Pathogenic forms of tau inhibit kinesin-dependent axonal transport through a mechanism involving activation of axonal phosphotransferases. J Neurosci 31:9858–9868.

Kondo M, Takei Y, Hirokawa N (2012) Motor protein KIF1A is essential for hippocampal synaptogenesis and learning enhancement in an enriched environment. Neuron 73:743–757.

Kwinter D, Silverman MA (2009) Live imaging of dense-core vesicles in primary cultured hippocampal neurons. J Vis Exp (27):1140.

Lambert MP, Barlow AK, Chromy BA, Edwards C, Freed R, Liosatos M, Morgan TE, Rozovsky I, Trommer B, Viola KL, Wals P, Zhang C, Finch CE, Krafft GA, Klein WL (1998) Diffusible, nonfibrillar ligands derived from Abeta1-42 are potent central nervous system neurotoxins. Proc Natl Acad Sci USA 95:6448–6453.

Lambert MP, Velasco PT, Chang L, Viola KL, Fernandez S, Lacor PN, Khuon D, Gong Y, Bigio EH, Shaw P, De Felice FG, Krafft GA, Klein WL (2007) Monoclonal antibodies that target pathological assemblies of Abeta. J Neurochem 100:23–35.

LaPointe NE, Morfini G, Pigino G, Gaisina IN, Kozikowski AP, Binder LI, Brady ST (2009) The amino terminus of tau inhibits kinesin-dependent axonal transport: implications for filament toxicity. J Neurosci Res 87:440–451.

Lazarov O, Morfini GA, Pigino G, Gadadhar A, Chen X, Robinson J, Ho H, Brady ST, Sisodia SS (2007) Impairments in fast axonal transport and motor neuron deficits in transgenic mice expressing familial Alzheimer's disease-linked mutant presenilin 1. J Neurosci 27:7011–7020.

Lee JR, Shin H, Ko J, Choi J, Lee H, Kim E (2003) Characterization of the movement of the kinesin motor KIF1A in living cultured neurons. J Biol Chem 278:2624–2629.

Lo KY, Kuzmin A, Unger SM, Petersen JD, Silverman MA (2011) KIF1A is the primary anterograde motor protein required for the axonal transport of dense-core vesicles in cultured hippocampal neurons. Neurosci Lett 491:168–173.

Mandelkow EM, Stamer K, Vogel R, Thies E, Mandelkow E (2003) Clogging of axons by tau, inhibition of axonal traffic and starvation of synapses. Neurobiol Aging 24:1079–1085.

Maqbool M, Mobashir M, Hoda N (2016) Pivotal role of glycogen synthase kinase-3: a therapeutic target for Alzheimer's disease. Eur J Med Chem 107:63–81.

Mariga A, Mitre M, Chao MV (2017) Consequences of brain-derived neurotrophic factor withdrawal in CNS neurons and implications in disease. Neurobiol Dis 97:73–79.

McDonald A, Fogarty S, Leclerc I, Hill EV, Hardie DG, Rutter GA (2010) Cell-wide analysis of secretory granule dynamics in three dimensions in living pancreatic beta-cells: evidence against a role for AMPK-dependent phosphorylation of KLC1 at Ser517/Ser520 in glucose-stimulated insulin granule movement. Biochem Soc Trans 38:205–208.

Minoshima S, Cross D (2008) In vivo imaging of axonal transport using MRI: aging and Alzheimer's disease. Eur J Nucl Med Mol Imaging 35 [Suppl 1]:S89–S92.

Miranda CJ, Braun L, Jiang Y, Hester ME, Zhang L, Riolo M, Wang H, Rao M, Altura RA, Kaspar BK (2012) Aging brain microenvironment decreases hippocampal neurogenesis through Wnt-mediated survivin signaling. Aging Cell 11:542–552.

Morfini G, Szebenyi G, Elluru R, Ratner N, Brady ST (2002) Glycogen synthase kinase 3 phosphorylates kinesin light chains and negatively regulates kinesin-based motility. EMBO J 21:281–293.

Morfini GA, Burns M, Binder LI, Kanaan NM, LaPointe N, Bosco DA, Brown RH Jr, Brown H, Tiwari A, Hayward L, Edgar J, Nave KA, Garberrn J, Atagi Y, Song Y, Pigino G, Brady ST (2009) Axonal transport defects in neurodegenerative diseases. J Neurosci 29:12776–12786.

Mórotz GM, Glennon EB, Greig J, Lau DHW, Bhembre N, Mattedi F, Muschalik N, Noble W, Vagnoni A, Miller CCJ (2019) Kinesin light chain-1 serine-460 phosphorylation is altered in Alzheimer's disease and regulates axonal transport and processing of the amyloid precursor protein. Acta Neuropathol Commun 7:200.

Padzik A, Deshpande P, Hollos P, Franker M, Rannikko EH, Cai D, Prus P, Mågård M, Westerlund N, Verhey KJ, James P, Hoogenraad CC, Coffey ET (2016) KIF5C S176 phosphorylation regulates microtubule binding and transport efficiency in mammalian neurons. Front Cell Neurosci 10:57.

Pigino G, Morfini G, Pelsman A, Mattson MP, Brady ST, Busciglio J (2003) Alzheimer's presenilin 1 mutations impair kinesin-based axonal transport. J Neurosci 23:4499–4508.

Ramser EM, Gan KJ, Decker H, Fan EY, Suzuki MM, Ferreira ST, Silverman MA (2013) Amyloid-β oligomers induce tau-independent disruption of BDNF axonal transport via calcineurin activation in cultured hippocampal neurons. Mol Biol Cell 24:2494–2505.

Rodrigues EM, Weissmiller AM, Goldstein LS (2012) Enhanced β-secretase processing alters APP axonal transport and leads to axonal defects. Hum Mol Genet 21:4587–4601.

Seifert B, Eckenstaler R, Rönicke R, Leschik J, Lutz B, Reymann K, Lessmann V, Brigadski T (2016) Amyloid-beta induced changes in vesicular transport of BDNF in hippocampal neurons. Neural Plast 2016:4145708.

Sleigh JN, Rossor AM, Fellows AD, Tosolini AP, Schiavo G (2019) Axonal transport and neurological disease. Nat Rev Neurol 15:691–703.

Soppina V, Norris SR, Dizaji AS, Kortus M, Veatch S, Peckham M, Verhey KJ (2014) Dimerization of mammalian kinesin-3 motors results in superprocessive motion. Proc Natl Acad Sci USA 111:5562–5567.

Stokin GB, Goldstein LS (2006) Axonal transport and Alzheimer's disease. Annu Rev Biochem 75:607–627.

Stokin GB, Lillo C, Falzone TL, Brusch RG, Rockenstein E, Mount SL, Raman R, Davies P, Masliah E, Williams DS, Goldstein LS (2005) Axonopathy and transport deficits early in the pathogenesis of Alzheimer's disease. Science 307:1282–1288.

Stokin GB, Almenar-Queralt A, Gunawardena S, Rodrigues EM, Falzone T, Kim J, Lillo C, Mount SL, Roberts EA, McGowan E, Williams DS, Goldstein LS (2008) Amyloid precursor protein-induced axonopathies are independent of amyloid-beta peptides. Hum Mol Genet 17:3474–3486.

Ullah S, Lin S, Xu Y, Deng W, Ma L, Zhang Y, Liu Z, Xue Y (2016) dbPAF: an integrative database of protein phosphorylation in animals and fungi. Sci Rep 6:23534.

Vagnoni A, Rodriguez L, Manser C, De Vos KJ, Miller CC (2011) Phosphorylation of kinesin light chain 1 at serine 460 modulates binding and trafficking of calsyntenin-1. J Cell Sci 124:1032–1042.

Weaver C, Leidel C, Szpankowski L, Farley NM, Shubeita GT, Goldstein LS (2013) Endogenous GSK-3/shaggy regulates bidirectional axonal transport of the amyloid precursor protein. Traffic 14:295–308.

Yonekawa Y, Harada A, Okada Y, Funakoshi T, Kanai Y, Takei Y, Terada S, Noda T, Hirokawa N (1998) Defect in synaptic vesicle precursor transport and neuronal cell death in KIF1A motor protein-deficient mice. J Cell Biol 141:431–441.

Yue Y, Sheng Y, Zhang HN, Yu Y, Huo L, Feng W, Xu T (2013) The CC1-FHA dimer is essential for KIF1A-mediated axonal transport of synaptic vesicles in *C. elegans*. Biochem Biophys Res Commun 435:441–446.

Zhang L, Trushin S, Christensen TA, Tripathi U, Hong C, Geroux RE, Howell KG, Poduslo JF, Trushina E (2018) Differential effect of amyloid beta peptides on mitochondrial axonal trafficking depends on their state of aggregation and binding to the plasma membrane. Neurobiol Dis 114:1–16.